Coupling of quantum-dot states via elastic cotunneling and crossed Andreev reflection in a minimal Kitaev chain

Zhi-Hai Liu [1,*] Chuanchang Zeng [1,†] and H. Q. Xu [2,1,‡]

[1]*Beijing Academy of Quantum Information Sciences*, Beijing 100193, China

[2]*Beijing Key Laboratory of Quantum Devices, Key Laboratory for the Physics and Chemistry of Nanodevices, and School of Electronics, Peking University, Beijing 100871, China*

We consider a quantum-dot (QD) based minimal Kitaev chain model and study the effects of modulation of QD states on the elastic cotunneling (ECT) and crossed Andreev reflection (CAR) processes. We demonstrate that the ECT amplitudes are strongly dependent on the energies of the QD states and are generally asymmetric, even in the absence of magnetic field, with respect to the chemical potential in the proximitized superconducting nanowire. We calculate the phase diagram of the total electron-number parity of the two QDs in terms of the spin-quantization axis direction in the QDs and the chemical potential in the superconducting nanowire, and also evaluate the precondition to attain a balance between ECT and CAR towards realizing the poor man's Majorana bound states. When the QDs are tuned into the deep Coulomb blockade regime, we predict a controllable anisotropic superexchange interaction between electrons in the two QDs under the combined effect of high-order interdot ECT and CAR processes.

I. INTRODUCTION

Semiconductor-superconductor hybrid nanostructures have recently attracted intensive attention for the exploration of nontrivial physical phenomena [1–4]. Attributed to strong spin-orbit interactions (SOIs) and large Landé-g factors of narrow-bandgap III-V semiconductors, superconducting nanowires have shown to be excellent platforms for the studies of the anomalous current-phase relations [5–9], superconducting diode effects [10–13], and Majorana bound states (MBSs) [14–16]. When coupled with the gate-defined quantum dots (QDs), superconducting nanowires can also enable the formation of superconducting spin qubits [17–23] and be exploited to build singlet or triplet Cooper-pair splitters [24–30]. More recently, it has been demonstrated that multiple QDs interconnected by a proximitized superconducting nanowire can effectively mimic a short Kitaev chain [31–37], in which MBSs can be presented in a poor man's manner [38,39]. In these burgeoning implementations with the QD-based Kitaev chains, the interactions between electrons in two separate QDs are found to be mediated by the Andreev bound states (ABSs) residing in the proximitized nanowire segments [28,38–41].

Theoretically, in the minimal Kitaev chain, the ABSs can facilitate interdot elastic-cotunneling (ECT) and crossed Andreev reflection (CAR) [40–42]. In addition, under the impact of SOI in the proximitized nanowire, both ECT and CAR can consist of spin-conserved and spin-flipped processes. In an initial QD-based Kitaev chain model [32], the effect of SOI

is not included and thus a fine tuning of local magnetic fields applied on the QDs is required to reach the sweet spot, thereby creating the poor man's MBSs. Motivated by the experiments reported in Refs. [28,41], the influence of SOI is explicitly included in recent theoretical treatments of Refs. [33,42] and the sweet spot can be reached by tuning the electric gates beneath the proximitized semiconductor nanowire segments. The underlying physics behind these theoretical treatments is tuning the spin-conserved and spin-flipped ECTs and CARs via SOI in the proximitized nanowire. However, these spin-dependent processes can also strongly depend on the energy states in the QDs. In fact, the constructions of poor man's MBSs [38,39], as well as Cooper-pair splitters [27–30], demand a strict control of the spin-dependent ECTs and CARs. This actually involves ascertainments of the QD electron states in addition to the direct couplings with the ABSs. Therefore, it remains a top priority to clarify the effect of the QD states along with their various modulations on the ABS-mediated CARs and ECTs in order to facilitate revealing the rich physics in the minimal Kitaev chain.

In this work, we analyze the ABS-mediated tunneling processes, namely, CARs and ECTs, by constructing a tight-binding (TB) model in close analogy to the experimental setup in Ref. [41], as schematically shown in Fig. 1. Instead of using phenomenal parameters, the coefficients of the direct couplings between QD states and ABSs are obtained from the localized states in each section. Utilizing the Schrieffer-Wolff transformation, we derive the analytical expressions for the amplitudes of spin-dependent ECTs and CARs between the two QDs. Remarkably, in contrast to the robustness of the CAR amplitudes, we find that the ECT amplitudes are strongly dependent on the energy of the QD states. Particularly, the average QD energy can be extracted from an

---

*Contact author: liuzh@baqis.ac.cn

†Contact author: zengcc@baqis.ac.cn
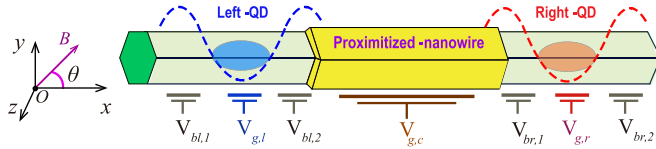
‡Contact author: hqxu@pku.edu.cn

FIG. 1. Schematic diagram of the two separate gate-defined quantum dots (QDs) interconnected by a superconducting proximitized nanowire, i.e., QD-based minimal Kitaev chain. Here, V is the gate potential, where subindex b (g) indicates barrier (plunger) gate, while l, c, r implies the left, center, and right sections, respectively. The applied magnetic field is also depicted as $\mathbf{B} = B(\cos\theta, \sin\theta, 0)$.

experimentally observed gate-tuning asymmetry of the ECTs in the absence of an external magnetic field [41]. With the change of the spin-quantization axis direction of the QDs in different but uniform magnetic fields, we also reveal that the balance of ECT and CAR in realizing poor man's MBSs is compatible with the emergence of fermion-parity degeneracy in low-energy states. We predict that when the QD energy levels are largely tuned below the Fermi level and deep in the Coulomb blockade regime, an anisotropic superexchange interaction between electrons in the two QDs can emerge under the combined effect of high-order ECT and CAR processes. Intriguingly, we also find this superexchange is highly tunable, which implies the capability of implementing two-qubit logic gates based on the minimal Kitaev chain model.

II. MODEL

The two separated QDs we consider are defined around the two ends of a semiconductor nanowire with strong Rashba SOI, e.g., InAs or InSb nanowire, with the connection section proximitized by a superconductor Al, as shown in Fig. 1. In the presence of a magnetic field $\mathbf{B} = B(\cos\theta, \sin\theta, 0)$ applied in the $x - y$ plane, the single-particle Hamiltonian of the hybrid nanowire along the x-axial direction reads as

$$H_e(x) = -\frac{\hbar^2}{2}\frac{\partial}{\partial x}\frac{1}{m_e(x)}\frac{\partial}{\partial x} + \frac{g(x)\mu_B}{2}\mathbf{B}\cdot\boldsymbol{\sigma} + V(x)$$
$$- i\frac{\hbar}{2}\left[\frac{\partial}{\partial x}\alpha(x) + \alpha(x)\frac{\partial}{\partial_x}\right]\sigma_y, \qquad (1)$$

where $m_e(x)$, $g(x)$, and $\alpha(x)$, respectively, correspond to the site-dependent electron effective mass (EMS), the Landé-g factor, and the Rashba SOI strength absorbing the partial metallization effect caused by the coated superconductor. $\boldsymbol{\sigma} = (\sigma_x, \sigma_y, \sigma_z)$ denotes the Pauli matrix vector, μ_B is the Born magneton, and $V(x)$ depicts the confinement potential induced by the gate voltages. In addition, a finite proximitized superconductivity can be induced in the middle section as $\Delta_s(x) = \Delta_0\Theta(w - |x|)$, with Δ_0 representing the induced superconducting gap, $\Theta(x)$ being a Heaviside function, and w the half-width of the proximitized section.

III. LOCALIZED CONFINED STATES

Without loss of generality, the local confinement potential of the left/right QD can be modeled as $V_{l/r}(x) = m_{e,0}\omega_0^2(x \pm d)^2/2 + V_{g,l/r}$, in which $m_{e,0/1}$ ($\alpha_{0/1}$ and $g_{0/1}$) quantifies the

specific value of the EMS (the SOI strength and Landé factor) in the bare/proximitized nanowire, ω_0 is the frequency of the harmonic potential, d is the half interdot distance, and $V_{g,l/r}$ is the relevant plunger-gate potential. In the case of $\Delta_{z,0} \equiv g_0\mu_B B \ll \hbar\omega_0$, the lowest Zeeman-splitting states of the QDs, $|\Psi_{l/r\Uparrow}\rangle$ and $|\Psi_{l/r\Downarrow}\rangle$ can be analytically derived by treating the Zeeman interaction as a perturbation [43,44]. Because the QDs are defined in the segments uncovered by superconductor Al, the obtained states are the normal electron states without superconducting correlation (SC). The intradot normal reflection and interference effects are automatically included in deriving the QD states, based on the continuous model as described in Eq. (1). The corresponding energies are given by $E_{\nu,\Uparrow/\Downarrow} = E_\nu \pm f_0(\theta)\Delta_{z,0}/2$ with $\nu = l, r$, in which $E_\nu = V_{g,\nu} + (\hbar\omega_0 - m_{e,0}\alpha_0^2)/2$ represents the effective orbital on-site energy, and $f_0(\theta) = (\sin^2\theta + e^{-2x_0^2/x_{so}^2}\cos^2\theta)^{1/2}$ is the SOI-induced modified factor of the Zeeman splitting, with $x_0 = [\hbar/(m_{e,0}\omega_0)]^{1/2}$ and $x_{so} = \hbar/(m_{e,0}\alpha_0)$. Here, because the intriguing physics we focused on occurs within the superconducting gap, which is much smaller than the orbital splitting energy of the QDs [42], the effect of high-energy QD states is not included in our model.

For the intermediate proximitized nanowire, the combination of the middle three applied gate potentials (cf. $V_{bl,2}$, $V_{g,c}$, and $V_{br,1}$ in Fig. 1), in principle, can also be endowed by a concave-shaped confinement, $V_{in}(x) = m_{e,1}\omega_1^2 x^2/2 + V_{g,c}$ with ω_1 specifying the parabolic potential. As such, the low-energy ABSs of the intermediate nanowire can be analytically derived based on the effective Hamiltonian $H_{BdG} = [p_x^2/(2m_{e,1}) + \alpha_1 p_x\sigma_y + V_{in}(x)]\tau_z + \Delta_0\tau_x + \Delta_{z,1}(\cos\theta\sigma_x + \sin\theta\sigma_y)/2$ [44], with $p_x = -i\hbar\partial/(\partial x)$, $\Delta_{z,1} = g_1\mu_B B$, and $\tau_{x,y,z}$ the Pauli matrices defining in the particle-hole (PH) space. The energies of the lowest two ABSs above the Fermi (zero-energy) level are

$$E_{1/2} = \sqrt{\mu^2 + \Delta_0^2} \pm \frac{f_1(\theta)}{2}\Delta_{z,c}, \qquad (2)$$

with $\mu = V_{g,c} + (\hbar\omega_1 - m_{e,1}\alpha_1^2)/2$ and $f_1(\theta)$ similar to $f_0(\theta)$ but with $m_{e,0}$, α_0 and ω_0 replaced by $m_{e,1}$, α_1 and ω_1, respectively. Equivalently, μ represents the effective chemical potential of the middle nanowire segment in the normal state, i.e., before including the SC correlation, which can be regulated using the plunger gate potential $V_{g,c}$ (see Fig. 1). The energies of the two ABSs below the Fermi level obey $E_{3/4} = -E_{2/1}$, in accordance with the PH symmetry of the BdG Hamiltonian $\mathcal{P}H_{BdG}\mathcal{P}^{-1} = -H_{BdG}$, with $\mathcal{P} = i\tau_y\sigma_y K$ and K being the PH and complex-conjugation operators. Indeed, because of the superconducting proximity effect, the ABSs emerge as quasi-particles and can be denoted by the Bogoliubov operators γ_j with $j = 1 - 4$, respectively.

The extension of the ABSs in the bare section will lead to direct tunnel couplings with the QD states [44]. In the language of second quantization, the corresponding TB Hamiltonian for the hybrid nanostructure is

$$H_{TB} = \sum_{\nu,s} E_{\nu,s}d_{\nu s}^\dagger d_{\nu s} + \sum_j E_j\gamma_j^\dagger\gamma_j$$
$$+ \sum_{\nu,s,j}(t_{\nu s,j}d_{\nu s}^\dagger\gamma_j + \text{H.c.}), \qquad (3)$$
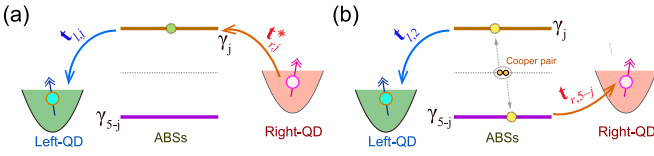
FIG. 2. Schematic diagram of ECT (a) and CAR (b). (a) depicts an electron quasi-spin-state transfer from the right QD to the left QD while (b) shows two electron states are created in them, which, respectively, mediated by the ABS γ_j and the PH-symmetric pair (γ_j, γ_{5-j}) of the middle hybrid nanowire. Here, $\mathbf{t}_{l(r),j} = \{t_{l(r)\Uparrow,j}, t_{l(r)\Downarrow,j}\}$ are the amplitude vectors of the direct tunnel couplings.

in which $d_{\nu s}^\dagger$ ($d_{\nu s}$) represents the creation (annihilation) operator for the QD state $|\Psi_{\nu,s}\rangle$ with $s = \Uparrow, \Downarrow$, and $t_{\nu s,j}$ characterizes the amplitude of the electron state tunnel coupling to the ABS γ_j. In addition to a structure-dependent (spinless) parameter t_0, specifically because of the SOI, the coupling amplitude also depend on the accumulated spin rotation phase $\Phi_{so} = \tilde{d}/x_{so}$ in the tunneling [44]. Note that, the effective length $\tilde{d}$ is different from the actual interdot distance d, due to the SOI inhomogeneity along the axial direction.

IV. EFFECTIVE INTERDOT INTERACTIONS

For the case of $E_{\nu,s} \ll |E_j|$, it is interesting to find the direct tunnel couplings with the intermediate ABSs can enable the ECT and CAR between electron states of the two separated QDs. In fact, this is accompanied by virtual excitations or evacuations of the middle higher- or lower-energy ABSs, as seen in Fig. 2. Explicitly, the effective Hamiltonian for the two long-range interactions are presented as $H_{\mathrm{ECT}} = \sum_{ss'=\Uparrow,\Downarrow}(d_{ls}^\dagger T_{ss'}d_{rs'} + \mathrm{H.c.})$ and $H_{\mathrm{CAR}} = \sum_{ss'}(d_{ls}^\dagger R_{ss'}d_{rs'}^\dagger + \mathrm{H.c.})$, with the spin-dependent amplitudes given by

$$T_{ss'} = \sum_{j=1-4} \frac{t_{ls,j}t_{rs',j}^*}{2}\left(\frac{1}{E_{l,s}-E_j} + \frac{1}{E_{r,s'}-E_j}\right),$$

$$R_{ss'} = \sum_{j=1-4} \frac{t_{ls,j}t_{rs',(5-j)}}{2}\left(\frac{1}{E_{l,s}-E_j} + \frac{1}{E_{(5-j)}-E_{r,s'}}\right). \quad (4)$$

Intuitively, ECT is achieved via the sequential single-electron (γ_j) transports, as seen in Fig. 2(a). In contrast, CAR involves the creation or annihilation of two electrons in the QDs, mediated by the PH-symmetric ABSs γ_j and γ_{5-j} originating from a Cooper pair [see Fig. 2(b)]. It is evident that the implementation of interdot ECT and CAR can also be mediated by other high-energy ABSs living in the middle superconducting nanowire segment. Quantitatively, by analogy with Eq. (4), the contributions of the high-energy ABSs are inversely proportional to their specific energy differences, with respect to the energies of the QD states involved in the processes. Thus, when the energy splitting of the ABSs $\hbar\omega_1 \gg \Delta_0$, the influences of these high-energy ABSs can be safely neglected, and our results are most appropriate to the case where only the four ABSs $\gamma_{j=1-4}$ are active in the superconducting gap.
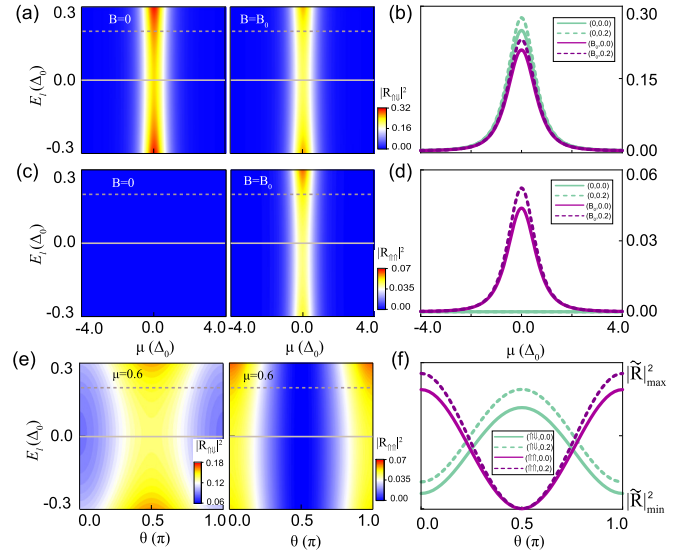

FIG. 3. The numerically calculated $|R_{\Uparrow\Downarrow}|^2$ (a) and $|R_{\Uparrow\Uparrow}|^2$ (b) in $\mu - E_l$ plane, with a zero ($B = 0$, left) and nonzero ($B = B_0$, right) magnetic field at $\theta = 0.25\pi$. (e) shows the variations of $|R_{\Uparrow\Downarrow}|^2$ (left) and $|R_{\Uparrow\Uparrow}|^2$ (right) versus θ and E_l, with $B = B_0$ and $\mu = 0.6\Delta_0$. The line cuts in (a), (c), and (e) are plotted in (b), (d) and (f), respectively, whose labels indicate the selected parameters from the colormaps. Range $[(|\tilde{R}|^2_{\max}, |\tilde{R}|^2_{\min})]$ in (f) implies the corresponding scales [0.08, 0.16] for $|R_{\Uparrow\Downarrow}|^2$ and [0.00, 0.06] for $|R_{\Uparrow\Uparrow}|^2$. Here, the values are presented in the unit of $4t_0^4/\Delta_0^2$, the nonzero magnetic field is $\Delta_{z,0} = 0.16\Delta_0$, the other system parameters are fixed as $E_r = 1.2E_l$, $\Delta_{z,c} = 0.5\Delta_{z,0}$, $\tilde{d} = 200$ nm, $x_{so} = 160$ nm, $x'_{so} \equiv \hbar/(m_e\alpha_1) = 240$ nm, $x_0 = 30$ nm, and $x_1 \equiv [\hbar/(m_e\omega_1)]^{1/2} = 70$ nm.

By noting the energy conservation warranted by the paired ABSs in $R_{ss'}$, i.e., $E_j + E_{5-j} \equiv 0$, the Hamiltonian for the CAR interaction can be effectively formulated as

$$H_{\mathrm{CAR}} = -\frac{t_0^2\Delta_0}{\mu^2 + \Delta_0^2}\begin{pmatrix}d_{l\Downarrow} \\ -d_{l\Uparrow}\end{pmatrix}^\dagger \hat{U}(2\Phi_{so})\begin{pmatrix}d_{r\Uparrow}^\dagger \\ d_{r\Downarrow}^\dagger\end{pmatrix} + \mathrm{H.c.}, \quad (5)$$

in which $\hat{U}(2\Phi_{so}) = \exp[-2i\Phi_{so}\hat{n}\cdot\boldsymbol{\sigma}]$ represents the spin rotation matrix induced by SOI, with the direction vector $\hat{n} = (\sin\vartheta, 0, \cos\vartheta)$ and $\vartheta = \arccos[\sin\theta/f_0(\theta)]$ [44]. In this form, the μ dependence of the amplitude $R_{ss'}$ is thus directly revealed by the coefficient of Eq. (5) now. Despite of the values of E_l and B, as shown in Fig. 3(a), $|R_{s\bar{s}}|^2$ manifests a rather robust dependency of μ, i.e., decreasing with increasing $|\mu|$, and always attain its maximum at $\mu = 0$ [see Fig. 3(b)]. Similar results for $|R_{ss}|^2$ are obtained, as plotted in Figs. 3(c) and 3(d), except at $B = 0$ where the spin-conserved CAR is suppressed because of the spin conservation [also see $\theta = \pi/2$ in Fig. 3(e)]. Specifically, Fig. 3(e) shows the numerical distributions of $|R_{ss}|^2$ and $|R_{s\bar{s}}|^2$ in the $\theta - E_l$ plane. Besides the evident dependence on direction angle θ in $\hat{n}$, it is seen that they are almost insensitive to the change of the energies of the QD states ($E_{l,r}$), as can be more clearly seen in Fig. 3(f). It is because of such insensitiveness, that the experimental observations of the main features for CARs in Ref. [41] can still be revealed by the current theoretical model even without specifying the QD energies in any detail (see Ref. [42]).
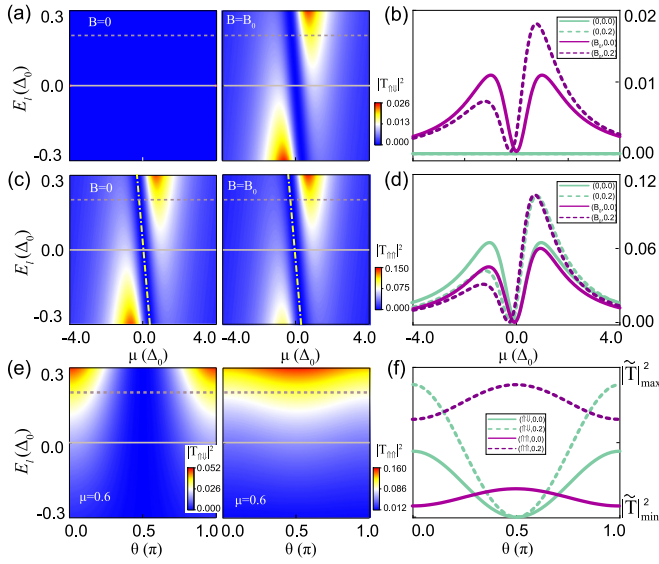
FIG. 4. Similar plots as in Fig. 3, but for the quantities $|T_{\Uparrow\Downarrow}|^2$ and $|T_{\Uparrow\Uparrow}|^2$, as shown by the color maps in the left and right columns, respectively; the corresponding line cut plots are also given in (b), (d), and (f). Note that, the white dashed-dotted lines in (c) indicate $|T_{\Uparrow\Uparrow}|^2 = 0$, and the scaling ranges $[(|\widetilde{T}|^2_{\min}, |\widetilde{T}|^2_{\max})]$ in (f) are now $[0.00, 0.04]$ and $[0.04, 0.12]$ for $|T_{\Uparrow\Downarrow}|^2$ and $|T_{\Uparrow\Uparrow}|^2$, respectively. Here, the used parameters are the same as those of Fig. 3.

Analytically, according to the specific forms of $t_{\nu s, j}$, $E_{\nu, s}$, and E_j, the ECT amplitude in Eq. (4) can be further evaluated by

$$
T_{ss'} = -\frac{t_0^2 (\mu + E_{ss'})}{\mu^2 + \Delta_0^2} [\hat{U}(-2\Phi_{so})]_{ss'} + \frac{t_0^2 \Delta_{z,c} f_1(\theta)}{2(\mu^2 + \Delta_0^2)}
$$
$$
\times \{ [\mathbf{\Pi}(\theta) \cdot \boldsymbol{\sigma}]_{ss'} + i\delta_{ss'} \sin(2\Phi_{so}) \cos\varphi \}, \quad (6)
$$

with $E_{ss'} = (E_{l,s} + E_{r,s'})/2$, $\delta_{ss'}$ being the Kronecker delta function, $\varphi = \arccos[\sin\theta / f_1(\theta)]$, and $\mathbf{\Pi}(\theta) = (\Pi_x, 0, \Pi_z)$ denoting a three-dimensional vector, with $\Pi_x = \cos^2\Phi_{so} \sin(\vartheta - \varphi) - \sin^2\Phi_{so} \sin(\vartheta + \varphi)$ and $\Pi_z = \cos^2\Phi_{so} \cos(\vartheta - \varphi) - \sin^2\Phi_{so} \cos(\vartheta + \varphi)$ [44].

In the absence or presence of an applied magnetic field, the intricate dependences of ECTs on the chemical potential of the middle superconducting nanowire were explicitly revealed in Ref. [41] at a fixed configuration of the QD energy levels. Admitted by the spin conservation in the absence of magnetic field, the spin-flipped ECTs are forbidden and hence we have $T_{s\bar{s}} = 0$, as shown in Fig. 4(a) for $B = 0$. Contrarily, Fig. 4(c) shows that the spin-conserved quantity $|T_{ss}|^2$ exhibits evident μ- and E_l dependences in this case. It is found $|T_{ss}|^2$ vanishes at $\mu \simeq -E_{ss}$ (see the dashed-dotted lines), accompanied with two local peaks emerging around. Interestingly, based on Eq. (6), the ratio of the two bilateral peak values at a fixed E_{ss} can be evaluated as

$$
\gamma_0 = (E_{ss} + \Delta_{es})^2 / (E_{ss} - \Delta_{es})^2, \quad (7)
$$

with $\Delta_{es} = (E_{ss}^2 + \Delta_0^2)^{1/2}$. Thus, it can be inferred that the spin-conserved probability is generically μ asymmetric. The predicted asymmetric trend, remarkably, can well capture the experimental observations in Ref. [41] [see Fig. 2(f) therein],

according to which estimations of $\gamma_0 \simeq 2.4$ and the average energy of the QD states $E_{ss} \simeq 0.22\Delta_0$ can also be extracted. This phenomenon can also be intuitively explained by an unbalance between the individual contributions from the positive ($\gamma_{1,2}$) and negative ($\gamma_{3,4}$) ABS levels and specifically, the utmost peak of the ECT rate is mainly contributed by the particular ABS levels nearer to the average energy of the QD states.

Note that, the asymmetric μ dependence of $|T_{ss}|^2$ can also appear when a magnetic field is applied, even when $E_{l,r} = 0$, see the (dark) solid line in Fig. 4(d) with $B = B_0$. Concurrently, spin-flipped ECTs come to play as verified by the data shown in the right panel of Fig. 4(a), and $|T_{s\bar{s}}|^2$ presenting a much similar μ and E_l dependences as that for $|T_{ss}|^2$ without magnetic field. For the case of a nonzero E_l, it is interesting to see that the variations of $|T_{s\bar{s}}|^2$ versus μ, as illustrated by the (dark) dashed curve in Fig. 4(b), can well explain the asymmetric feature of the spin-flipped probability measured in the experiments [refer to Fig. 3(d) of Ref. [41]]. Evidently, based on Eq. (6), the spin-dependent ECT amplitudes will also vary with the magnetic-field direction in different values of the QD energies. As shown in Figs. 4(e) and 4(f), $|T_{s\bar{s}}|^2$ and $|T_{ss}|^2$ attain their local maxima and minima at $\theta = 0, \pi$, respectively. In contrast to that for CARs in Fig. 3(e) and 3(f), apparently, they exhibit significant modulations by the QD energies.

V. MORE PHYSICS RELATES TO QD ENERGIES

Being as a zero-energy and half-fermionic state, it is confirmed that the emergence of a pair of poor man's MBSs can be indicated by the fermion parity degeneracy in the low-energy states [33,35], when the on-site energies of the two QDs are symmetrically kept around the Fermi level. However, it still remains an open question to clarify the impact of modulation of the spin-quantization axis direction of the QDs on the precondition for realizing the MBSs in a minimal Kitaev chain.

With the change of the spin quantization-axis direction in different but uniform magnetic fields, Fig. 5(a) shows the parity phase diagram of the total electron-number parity of the two QDs in the $\theta - \mu$ plane, where, for completeness, the effect of intradot Coulomb repulsions is also included in the calculation [44]. Clearly, for a fixed magnetic-field direction θ, the fermion parity of the double QDs is even when the chemical potential of the superconducting nanowire μ is kept within a range around the zero-energy level, and it will change to be odd as μ out of the range. The boundary between the odd and even fermion parity areas indicates the correlation of the two modulation parameters required to attain the parity degeneracy. Intriguingly, this is consistent with the conventional criteria for the poor man's MBSs in Ref. [32], where a balance between the interdot spin-conserved ECT and CAR $|T_{\Downarrow\Downarrow}|^2 = |R_{\Downarrow\Downarrow}|^2$ is necessary. Note that, because of the vanishing of spin-conserved CARs at $\theta = \pi/2$ [see Fig. 3(f)], the emergence of parity degeneracy does not really ensure the creation of the MBSs, as indicated by the deviation emerging there in Fig. 5(a).

When the QD energies are considerably tuned below the Fermi level and with $\Delta_{z,0} \ll |E_{l,r}|$, the QDs are deep
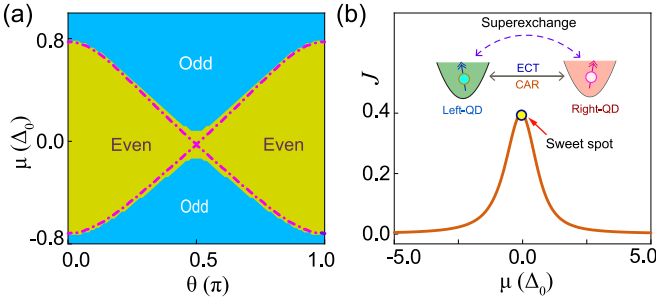
FIG. 5. (a) The phase diagram of the total electron-number parity of the two QDs in the $\theta - \mu$ plane, with $E_{l,r} = 0.1$, $\Delta_{z,0} = 0.2$, $U = 5.0$. Here, these energy scales are in units of Δ_0, and the other parameters take the same values as that in Fig. 3. The dotted-dashed curves (purple) indicate the required $\theta - \mu$ correlation for $|T_{\downarrow\downarrow}|^2 = |R_{\downarrow\downarrow}|^2$. (b) The numerically calculated superexchange (see the inset) interaction strength J based on Eq. (8), in a unit of $8t_0^4/\Delta_0^3$, as a function of μ, for the double QDs. Here we have $E_l = -0.3$, $E_r = -0.4$, and $\Delta_{z,0} = 0.05$, and a sweet spot is also presented.

in the even-parity phase regime and characterized by the (1,1) occupancy distribution, i.e., each QD occupied by a single electron. Nevertheless, within the strong Coulomb blockade regime, i.e., $|E_{\nu,s}|, |E_j| \ll U$ with U sizing the strength of the Coulomb repulsion, the electrons of the two QDs will establish an effective exchange interaction under the combined effect of high-order interdot ECT and CAR processes. Using the explicit forms of the spin-dependent amplitudes given in Eqs. (5) and (6), the exchange Hamiltonian is found as, $\mathcal{H}_{\text{ext}} = J[\cos^2(2\Phi_{\text{so}})\mathbf{S}_l \cdot \mathbf{S}_r + \sin(4\Phi_{\text{so}})\hat{n} \cdot (\mathbf{S}_l \times \mathbf{S}_r) + \sin^2(2\Phi_{\text{so}})\mathbf{S}_l \overleftrightarrow{\Gamma} \mathbf{S}_r]$ [44]. Here, we have $\overleftrightarrow{\Gamma} = 2\hat{n}\hat{n} - 1$, $\mathbf{S}_{\nu=l,r} = (1/2)\sum_{s,s'} d^{\dagger}_{\nu s'}\boldsymbol{\sigma}_{s's}d_{\nu s}$ representing the electron quasi-spin operators and

$$J = \frac{t_0^4 U}{(\mu^2 + \Delta_0^2)^2}\left[\frac{(2\mu + E_+)^2}{U^2 - E_-^2} - \frac{4\Delta_0^2}{E_+(2U + E_+)}\right], \quad (8)$$

indicating the strength of the exchange interaction, with $E_{\pm} = E_l \pm E_r$.

In contrast to the formation of MBSs around the Fermi level [31,32], the exchange interaction is established only when the on-site energies of the QDs are significantly reduced below the zero-energy level. As described by the effective Hamiltonian $\mathcal{H}_{\text{ext}}$, it not only comprises a generic Heisenberg exchange interaction but also contains an anisotropic Dzyaloshinskii-Moriya (DM) interaction and a symmetric ferromagnetic term, namely as a superexchange interaction [46,47]. Interestingly, the direction of the DM vector in $\mathcal{H}_{\text{eff}}$, viz., $\hat{n}$, vary with the direction of the magnetic field and

the exchange strength J can be regulated by the chemical potential μ, as shown in Fig. 5(b). Specifically, when μ is tuned approaching to (away from) the zero point, J is effectively switched on (off) with the modulation reaching a sweet point of $\partial J/\partial\mu = 0$. The emergence of a controllable superexchange interaction will facilitate the spin-based quantum computation in the minimal Kitaev chain, because the implementation of intrinsic two-qubit logic gates demands for a tunable superexchange interaction [48–50].

VI. CONCLUSION

Focusing on the interaction between two separated QDs mediated by the ABSs of a superconducting proximitized nanowire, we clarify different interesting effects on the ECTs and CARs from tuning the energies of the QD states, as explicitly considered in our model. Regarding the CARs, we demonstrate that the modulation of energy levels of the QDs does not affect the respective spin-dependent amplitudes. This validates the physical rationality of the simplified treatment in Ref. [42] in analyzing CARs, in which the details of the QD states are not explicitly accounted for. Contrastingly, the ECT amplitudes exhibit an evident dependence on the QD energies, and thus illustrate the insufficiency of the existing theory in interpreting the experimentally observed gate-tuning asymmetry of ECTs in the case without magnetic field [41].

Armed with the variation laws of the spin-dependent ECTs and CARs, we derive the phase diagram of the total electron-number parity of the two QDs in terms of the spin-quantization axis direction in the QDs and the chemical potential in the superconducting nanowire, and demonstrate that the emergence of a fermion-parity degeneracy is compatible with a balance between ECT and CAR in realizing the poor man's MBSs. When the QDs are tuned into the deep Coulomb blockade regime and kept at half-filling, we also predict an anisotropic superexchange interaction between electrons of the two QDs under the impact of high-order ECT and CAR processes. In addition, the high controllability of the superexchange interaction will facilitate implementing two-qubit logic gates based on the electron spin states. Overall, we believe our work elucidates a more complete picture of the modulation of spin-dependent ECTs and CARs in the QD-based minimal Kitaev chain, and will invoke more interesting physics studies in the superconducting hybrid QD nanostructures.

[1] G. Burkard, M. J. Gullans, X. Mi, and J. R. Petta, Superconductor-semiconductor hybrid-circuit quantum electrodynamics, Nat. Rev. Phys. **2**, 129 (2020).

[2] K. Flensberg, F. von Oppen, and A. Stern, Engineered platforms for topological superconductivity and Majorana zero modes, Nat. Rev. Mater. **6**, 944 (2021).

[3] S. M. Frolov, M. J. Manfra, and J. D. Sau, Topological super-conductivity in hybrid devices, Nat. Phys. **16**, 718 (2020).

[4] R. M. Lutchyn, E. P. A. M. Bakkers, L. P. Kouwenhoven, P. Krogstrup, C. M. Marcus, and Y. Oreg, Majorana zero modes in superconductor-semiconductor heterostructures, Nat. Rev. Mater. **3**, 52 (2018).

[5] A. Zazunov, R. Egger, T. Jonckheere, and T. Martin, Anomalous Josephson Current through a spin-orbit coupled quantum dot, Phys. Rev. Lett. **103**, 147004 (2009).

[6] E. M. Spanton, M. Deng, S. Vaitiekenas, P. Krogstrup, J. Nygård, C. M. Marcus, and K. A. Moler, Current-phase relations of few-mode InAs nanowire Josephson junctions, Nat. Phys. **13**, 1177 (2017).

[7] D. B. Szombati, S. Nadj-Perge, D. Car, S. R. Plissard, E. P. A. M. Bakkers, and L. P. Kouwenhoven, Josephson ϕ_0-junction in nanowire quantum dots, Nat. Phys. **12**, 568 (2016).

[8] D. Laroche, D. Bouman, D. J. van Woerkom, A. Proutski, C. Murthy, D. I. Pikulin, C. Nayak, R. J. J. van Gulik, J. Nygård, P. Krogstrup, L. P. Kouwenhoven, and A. Geresdi, Observation of the 4π-periodic Josephson effect in indium arsenide nanowires, Nat. Commun. **10**, 245 (2019).

[9] V. Levajac, H. Barakov, G. P. Mazur, N. van Loo, L. P. Kouwenhoven, Y. V. Nazarov, and J.-Y. Wang, Supercurrent in the presence of direct transmission and a resonant localized state, Phys. Rev. Lett. **132**, 176304 (2024).

[10] M. Nadeem, M. S. Fuhrer, and X. Wang, The superconducting diode effect, Nat. Rev. Phys. **5**, 558 (2023).

[11] H. F. Legg, D. Loss, and J. Klinovaja, Superconducting diode effect due to magnetochiral anisotropy in topological insulators and Rashba nanowires, Phys. Rev. B **106**, 104501 (2022).

[12] T. Yokoyama, M. Eto, and Y. V. Nazarov, Anomalous Josephson effect induced by spin-orbit interaction and Zeeman effect in semiconductor nanowires, Phys. Rev. B **89**, 195407 (2014).

[13] H. Su, J.-Y. Wang, H. Gao, Y. Luo, S. Yan, X. Wu, G. Li, J. Shen, L. Lu, D. Pan, J. Zhao, P. Zhang, and H. Q. Xu, Microwave-assisted unidirectional superconductivity in Al-InAs nanowire-Al junctions under magnetic fields, Phys. Rev. Lett. **133**, 087001 (2024).

[14] R. M. Lutchyn, J. D. Sau, and S. Das Sarma, Majorana fermions and a topological phase transition in semiconductor-superconductor heterostructures, Phys. Rev. Lett. **105**, 077001 (2010).

[15] Y. Oreg, G. Refael, and F. von Oppen, Helical liquids and Majorana bound states in quantum wires, Phys. Rev. Lett. **105**, 177002 (2010).

[16] Microsoft Azure Quantum, Interferometric single-shot parity measurement in an InAs-Al hybrid device, arXiv:2401.09549.

[17] M. Hays, V. Fatemi, D. Bouman, J. Cerrillo, S. Diamond, K. Serniak, T. Connolly, P. Krogstrup, J. Nygård, A. Levy Yeyati, A. Geresdi, and M. H. Devoret, Coherent manipulation of an Andreev spin qubit, Science **373**, 430 (2021).

[18] C. Padurariu and Yu. V. Nazarov, Theoretical proposal for superconducting spin qubits, Phys. Rev. B **81**, 144519 (2010).

[19] M. Pita-Vidal, A. Bargerbos, R. Zitko, L. J. Splitthoff, L. Grunhaupt, J. J. Wesdorp, Y. Liu, L. P. Kouwenhoven, R. Aguado, B. van Heck, A. Kou, and C. K. Andersen, Direct manipulation of a superconducting spin qubit strongly coupled to a transmon qubit, Nat. Phys. **19**, 1110 (2023).

[20] A. P. Higginbotham, S. M. Albrecht, G. Kirsanskas, W. Chang, F. Kuemmeth, P. Krogstrup, T. S. Jespersen, J. Nygård, K. Flensberg, and C. M. Marcus, Parity lifetime of bound states in a proximitized semiconductor nanowire, Nat. Phys. **11**, 1017 (2015).

[21] T. W. Larsen, K. D. Petersson, F. Kuemmeth, T. S. Jespersen, P. Krogstrup, J. Nygård, and C. M. Marcus, Semiconductor-nanowire-based superconducting qubit, Phys. Rev. Lett. **115**, 127001 (2015).

[22] M. Spethmann, S. Bosco, A. Hofmann, J. Klinovaja, and D. Loss, High-fidelity two-qubit gates of hybrid superconducting-semiconducting singlet-triplet qubits, Phys. Rev. B **109**, 085303 (2024).

[23] M. Spethmann, X.-P. Zhang, J. Klinovaja, and D. Loss, Coupled superconducting spin qubits with spin-orbit interaction, Phys. Rev. B **106**, 115411 (2022).

[24] M.-S. Choi, C. Bruder, and D. Loss, Spin-dependent Josephson current through double quantum dots and measurement of entangled electron states, Phys. Rev. B **62**, 13569 (2000).

[25] R. S. Deacon, A. Oiwa, J. Sailer, S. Baba, Y. Kanai, K. Shibata, K. Hirakawa, and S. Tarucha, Cooper pair splitting in parallel quantum dot Josephson junctions, Nat. Commun. **6**, 7446 (2015).

[26] F. Brange, K. Prech, and C. Flindt, Dynamic cooper pair splitter, Phys. Rev. Lett. **127**, 237701 (2021).

[27] Q. Wang, S. L. D. ten Haaf, I. Kulesh, D. Xiao, C. Thomas, M. J. Manfra, and S. Goswami, Triplet correlations in Cooper pair splitters realized in a two-dimensional electron gas, Nat. Commun. **14**, 4876 (2023).

[28] G. Wang, T. Dvir, G. P. Mazur, C.-X. Liu, N. van Loo, S. L. D. ten Haaf, A. Bordin, S. Gazibegovic, G. Badawy, E. P. A. M. Bakkers, M. Wimmer, and L. P. Kouwenhoven, Singlet and triplet Cooper pair splitting in hybrid superconducting nanowires, Nature (London) **612**, 448 (2022).

[29] O. Kürtössy, Z. Scherübl, G. Fülöp, I. E. Lukács, T. Kanne, J. Nygård, P. Makk, and S. Csonka, Parallel InAs nanowires for Cooper pair splitters with Coulomb repulsion, npj Quantum Mater. **7**, 88 (2022).

[30] A. Bordoloi, V. Zannier, L. Sorba, C. Schönenberger, and A. Baumgartner, Spin cross-correlation experiments in an electron entangler, Nature (London) **612**, 454 (2022).

[31] J. D. Sau and S. Das Sarma, Realizing a robust practical Majorana chain in a quantum-dot-superconductor linear array, Nat. Commun. **3**, 964 (2012).

[32] M. Leijnse and K. Flensberg, Parity qubits and poor man's Majorana bound states in double quantum dots, Phys. Rev. B **86**, 134528 (2012).

[33] A. Tsintzis, R. S. Souto, and M. Leijnse, Creating and detecting poor man's Majorana bound states in interacting quantum dots, Phys. Rev. B **106**, L201404 (2022).

[34] C.-X. Liu, H. Pan, F. Setiawan, M. Wimmer, and J. D. Sau, Fusion protocol for Majorana modes in coupled quantum dots, Phys. Rev. B **108**, 085437 (2023).

[35] A. Tsintzis, R. S. Souto, K. Flensberg, J. Danon, and M. Leijnse, Majorana qubits and non-abelian physics in quantum dot-based minimal kitaev chains, PRX Quantum **5**, 010323 (2024).

[36] W. Samuelson, V. Svensson, and M. Leijnse, Minimal quantum dot based Kitaev chain with only local superconducting proximity effect, Phys. Rev. B **109**, 035415 (2024).

[37] R. S. Souto, A. Tsintzis, M. Leijnse, and J. Danon, Probing Majorana localization in minimal Kitaev chains through a quantum dot, Phys. Rev. Res. **5**, 043182 (2023).

[38] T. Dvir, G. Wang, N. van Loo, C.-X. Liu, G. P. Mazur, A. Bordin, S. L. D. ten Haaf, J.-Y. Wang, D. van Driel, F. Zatelli, X. Li, F. K. Malinowski, S. Gazibegovic, G. Badawy, E. P. A. M. Bakkers, M. Wimmer, and L. P. Kouwenhoven, Realization of a minimal Kitaev chain in coupled quantum dots, Nature (London) **614**, 445 (2023).

[39] A. Bordin, C.-X. Liu, T. Dvir, F. Zatelli, S. L. D. ten Haaf, D. van Driel, G. Wang, N. van Loo, T. van Caekenberghe, J. C. Wolff, Y. Zhang, G. Badawy, S. Gazibegovic, E. P. A. M. Bakkers, M. Wimmer, L. P. Kouwenhoven, and G. P. Mazur, Signatures of Majorana protection in a three-site Kitaev chain, arXiv:2402.19382.

[40] A. Bordin, X. Li, D. van Driel, J. C. Wolff, Q. Wang, S. L. D. ten Haaf, G. Wang, N. van Loo, L. P. Kouwenhoven, and T. Dvir, Crossed Andreev reflection and elastic cotunneling in three quantum dots coupled by superconductors, Phys. Rev. Lett. **132**, 056602 (2024).

[41] A. Bordin, G. Wang, C.-X. Liu, S. L. D. ten Haaf, N. van Loo, G. P. Mazur, D. Xu, D. van Driel, F. Zatelli, S. Gazibegovic, G. Badawy, E. P. A. M. Bakkers, M. Wimmer, L. P. Kouwenhoven, and T. Dvir, Tunable crossed andreev reflection and elastic cotunneling in hybrid nanowires, Phys. Rev. X **13**, 031031 (2023).

[42] C.-X. Liu, G. Wang, T. Dvir, and M. Wimmer, Tunable superconducting coupling of quantum dots via Andreev bound states in semiconductor-superconductor nanowires, Phys. Rev. Lett. **129**, 267701 (2022).

[43] R. Li, J. Q. You, C. P. Sun, and F. Nori, Controlling a nanowire spin-orbit qubit via electric-dipole spin resonance, Phys. Rev. Lett. **111**, 086805 (2013).

[44] See Supplemental Material at http://link.aps.org/supplemental/10.1103/PhysRevB.110.115302 for details of the two-sided QD states and the middle ABSs, the derivations of the tight-binding Hamiltonian H_{TB} in Eq. (3) and the ECT and CAR amplitudes $T_{ss'}$ and $R_{ss'}$, as well as the ascertainment of the parity of the ground state of the double QDs and the effective superexchange interaction in the strong Coulomb repulsion regime, which also includes Ref. [45].

[45] R. Winkler, *Spin-orbit Coupling Effects in Two-dimensional Electron and Hole Systems* (Springer, Berlin, 2003).

[46] Z.-H. Liu, O. Entin-Wohlman, A. Aharony, and J. Q. You, Control of the two-electron exchange interaction in a nanowire double quantum dot, Phys. Rev. B **98**, 241303(R) (2018).

[47] L. Shekhtman, O. Entin-Wohlman, and A. Aharony, Moriya's anisotropic superexchange interaction, frustration, and Dzyaloshinsky's weak ferromagnetism, Phys. Rev. Lett. **69**, 836 (1992).

[48] L.-A. Wu and D. A. Lidar, Universal quantum logic from Zeeman and anisotropic exchange interactions, Phys. Rev. A **66**, 062314 (2002).

[49] J. Klinovaja, D. Stepanenko, B. I. Halperin, and D. Loss, Exchange-based CNOT gates for singlet-triplet qubits with spin-orbit interaction, Phys. Rev. B **86**, 085423 (2012).

[50] J. Qi, Z.-H. Liu, and H. Q. Xu, Spin-orbit interaction enabled high-fidelity two-qubit gates, New J. Phys. **26**, 013012 (2024).